Support information

FeNiP Nanoparticle / N, P Dual-Doped Carbon Composite as a Trifunctional Catalyst towards High-Performance Zinc-Air Battery and Overall Water Electrolysis

Wendi Chen, Shengming Chang, Heping Yu, Wenming Li, Hui Zhang, Zhongyi Zhang*

College of Chemistry and Chemical Engineering, Qingdao University, Qingdao, 266071, P. R. China

** Corresponding author at: 507 Laboratory in Shen-Si building of Qingdao University, NO.7 East Hong Kong Road, Qingdao, Shandong, 266071, P. R. China. TEL: +86 13583203984. E-mail: Zhangzy@qdu.edu.cn*

Additional experimental section

Physicochemical characterizations

The X-ray diffraction pattern (XRD) was obtained on a Bruker D8 Advance X-ray diffractometer with Cu Kα radiation (λ=0.154 nm), with a scanning speed of 4°/min and a diffraction angle (2θ) ranging from 10 to 90°. The FEI Nova nano450 instrument was

used to record the scanning electron microscope (SEM) to study the microscopic morphology of the prepared catalyst. In order to further study the microscopic morphological element composition and distribution of the prepared catalyst, the FEI TALOS F200S instrument was used to record the transmission electron microscope (TEM) image, high power transmission electron microscope (HERTEM) images, and the Bruker QUANTAX instrument to record the high-angle circle Dark field scanning transmission electron microscope (HAADF) image and energy dispersive X-ray spectroscopy (EDS). The Quanta Autosorb-iQ analyzer was used to study the specific surface area and pore structure characteristics of the prepared catalyst under the paint surface, and the nitrogen adsorption and desorption experiments were carried out. The pore structure ranges from 0 to 50 nm. Raman spectra were obtained using Renishaw 1500080S instrument to investigate the graphitization differences and defects of the prepared catalysts. The test range was 0 to 4000 cm^{-1}. Find disordered carbon (D band) and ordered graphitic carbon (G band) through the obtained data. A Thermofisher ESCALAB 250Xi instrument was used to obtain the elemental composition and content of the catalyst prepared by the XPS X-ray Electronic Spectroscopy Institute. The binding energy was corrected according to the C1s peak at 284.8 eV, and the corresponding peak was fitted according to the XPS database and literature.

Electrochemical measurements

The catalytic activities of all the catalysts for the HER, ORR and OER performance were investigated with a CHI 760E electro-chemical workstation in a standard three-electrode system using an Ag/AgCl electrode as the reference electrode, a Pt electrode as the counter electrode, and a rotating disk electrode coated with the catalysts as the working electrode. The catalyst ink was prepared by dispersing 5 mg of the samples into 50 μl ethanol and 50 μl Nafion solution (5 wt%) and 900 μl deionized water. After ultraphonic for 30 min, 10 μl of the catalyst ink was deposited onto a 4 mm diameter polished glassy carbon electrode with a mass loading of 0.4 mg cm^{-2} and dried at room temperature. For comparison, Pt/C was used as a reference for the ORR and HER, while RuO_2 was used as a reference for the OER.

(1) The cyclic voltammetry test (CV) is carried out in 0.1 M KOH solution saturated with N_2 or O_2, the scan rate is 10 mV s^{-1}, and the gas introduction time is 15 minutes before the test. This article tests 3 circles of CV curve, using Data processing in the third circle.

(2) The ORR rotating disc test is carried out in 0.1 M KOH solution saturated with O_2, the scanning rate is 10 mV s^{-1}, and the linear scanning curve LSV is obtained at 1600 rpm.

The K-L equation is applied to investigate the ORR exact kinetic parameters. The K-L equation can be described as follows:

$$1/J = 1/J_l + 1/J_k = 1/B\omega^{1/2} + 1/J_k \quad (1)$$

$$B = 0.2nFC_0(D_0)^{2/3}\nu^{-1/6} \quad (2)$$

$$j_k = nFkC_0 \quad (3)$$

where J is the current density, J_k is the kinetic current density, ω is the rotation speed, n is the transferred electron number, F is the Faraday constant (F = 96485 C mol^{-1}), C_0 is the saturated concentration of oxygen in the electrolyte (1.21×10^{-3} mol l^{-1}), D_0 is the diffusion coefficient of oxygen in the solution (1.9×10^{-5} cm s^{-1}), υ is the kinetic viscosity of the electrolyte (0.01 cm2 s^{-1}), and k is the electron-transfer rate constant.

(3) The Rotating Ring Disk Electrode Test (RRDE) was carried out in 0.1 M KOH solution saturated with O_2 at 1600 rpm. The H_2O_2 yield calculated based on the RRDE data and the number of electrons per oxygen molecule transfer technique as follows:

$$H_2O_2(\%) = 200 * \frac{\frac{I_R}{N}}{I_D + \frac{IR}{N}} \quad (4)$$

$$n = 4 * \frac{\frac{I_R}{N}}{I_D + \frac{IR}{N}} \quad (5)$$

Where I_D is the disk current, I_R is the ring disk current, and N is the current collection rate of the Pt ring (N is equal to 0.43).

(4) The double-layer capacitance test is performed in 0.1 M KOH solution at a scan rate of 10, 30, 50, 70 and 90 mV s^{-1}, and the curve is drawn at a potential of 1.027V. The curve is drawn with the scan rate as the abscissa and the current density difference ($\Delta j = j_a - j_b$) at a fixed overpotential as the ordinate. The value of the slope of the drawing is twice that of C_{dl}.

(5) Electrochemical impedance spectroscopy (EIS) is tested in 1 M KOH solution. The current density of HER is -10 mA cm^{-2} and the current density of OER is 10 mA cm^{-2}, and the electrochemical impedance test is carried out in the frequency range of 0.01 Hz to 100 KHz with 5 mV amplitude.

ORR: 0.1 M KOH solution bubbled with oxygen was used as the electrolyte. The LSV curves were recorded at different rotation speeds of 400, 625, 900, 1225, 1600 and 2025 rpm at a scan rate of 10 mV s^{-1}. The durability was obtained by recording the chronoamperometry (i–t) curve at 1600 rpm.

OER: 1 M KOH solution bubbled with oxygen was used as the electrolyte. The LSV curves were recorded at 1600 rpm at a scan rate of 10 mV s^{-1}. The stability was obtained by recording the chronoamperometry (i-t) curve at 1600 rpm.

HER: 1 M KOH solution bubbled with N_2 was used as the electrolyte. The LSV curves were recorded at a scan rate of 10 mV s^{-1}.

The stability was obtained by recording the chronoamperometry (i-t) curve at 1600 rpm. All the potentials in this study were iRcorrected and converted to the RHE scale using the Nernstequation ($E_{RHE}=E_{Ag/AgCl}+ E^{\theta}_{Ag/AgCl}+ 0.059$ pH).

Battery assembly and test

Liquid Zn−Air Battery Assembly

The liquid Zn−air battery was assembled with catalyst-coated carbon cloth as the air cathode, a polished Zn plate as the anode, and 6.0 M KOH containing 0.2 M zinc acetate aqueous solution as the electrolyte. The air cathode was prepared by FeNiP@C-200 Ink onto carbon cloth with the catalyst loading of 1 mg cm^{-2} and drying at room temperature. For the assembly of a control battery, a commercial catalyst (20 wt % Pt/C: RuO_2= 1:1, mass ratio) was used with the same loading amount.

Flexible All-Solid-State Zn−Air Battery Assembly

The flexible all-solid-state Zn−air battery was assembled with the FeNiP@C-200-coated carbon cloth as the air cathode, a polished Zn foil (0.30 mm thickness) as the anode, and the gel polymer electrolyte as the electrolyte. The air electrode was made by dropping a certain volume of FeNiP@C-200 ink onto a clean carbon cloth substrate with a catalyst loading of 1 mg cm^{-2}.

Battery performance test

The discharge/charge tests were conducted using an automatic battery testing system (LANHE CT2001A). The specific capacity and energy density were calculated from the galvanostatic discharge and normalized to the mass of consumed zinc.

Particle size histogram

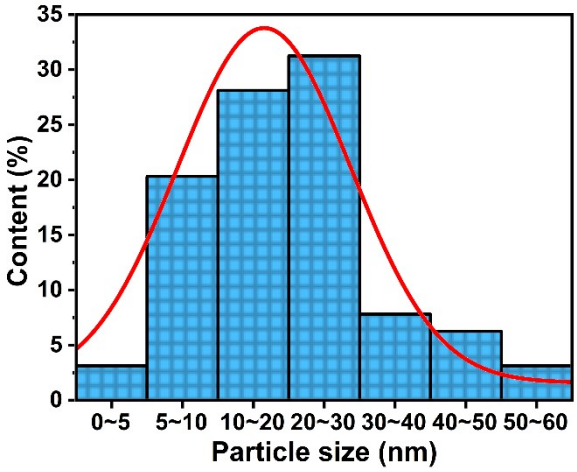

Fig. S1. A histogram of the particle size distribution diagram in Fig. 2b.

Specific surface area and pore structure

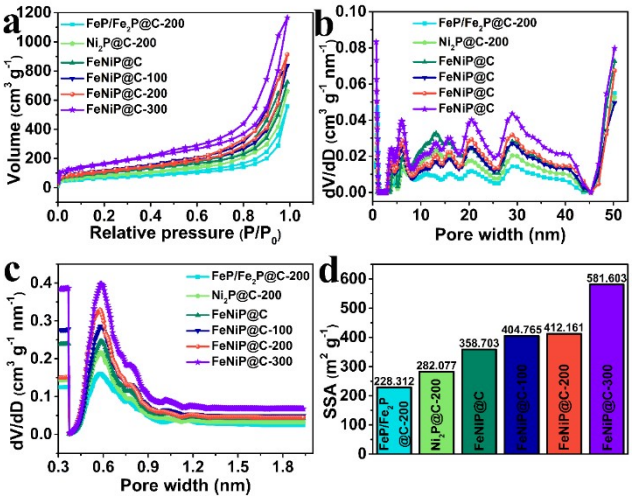

Fig. S2. (a) N_2 adsorption/desorption isotherm of FeP/Fe_2P@C-200, Ni_2P@C-200, FeNiP@C, FeNiP@C-100, FeNiP@C-200, FeNiP@C-300. (b) Pore size distribution of FeP/Fe_2P@C-200, Ni_2P@C-200, FeNiP@C, FeNiP@C-100, FeNiP@C-200 and FeNiP@C-300, (c) Micro-pore size distribution of FeP/Fe_2P@C-200, Ni_2P@C-200, FeNiP@C, FeNiP@C-100, FeNiP@C-200 and FeNiP@C-300. (d) Histogram of specific surface area of FeP/Fe_2P@C-200, Ni_2P@C-200, FeNiP@C, FeNiP@C-100, FeNiP@C-200 and FeNiP@C-300.

Additional results of XPS spectra

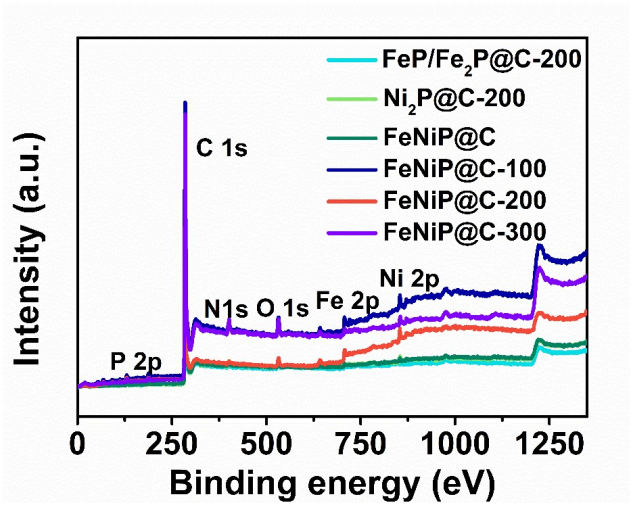

Fig. S3. XPS survey spectra of the FeP/Fe_2P@C-200, Ni_2P@C-200, FeNiP@C, FeNiP@C-100, FeNiP@C-200 and FeNiP@C-300 samples.

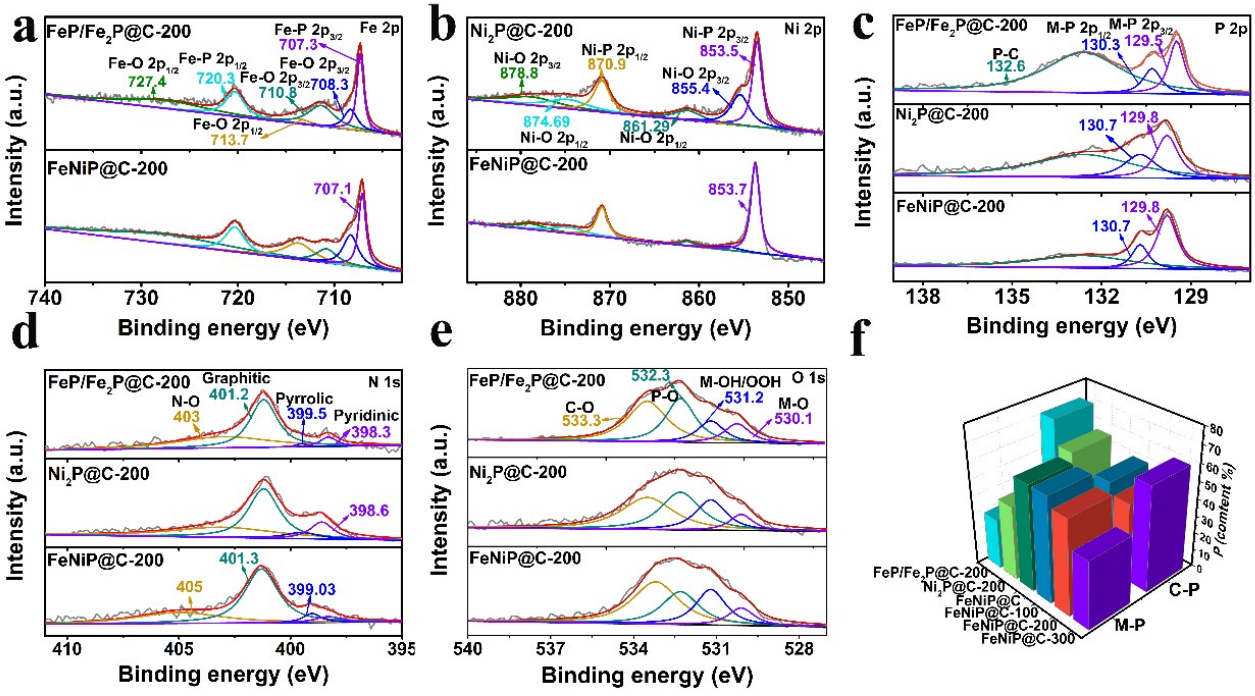

Fig. S4. XPS of FeP/Fe_2P@C-200, Ni_2P@C-200, FeNiP@C-200 (a) Fe 2p, (b) Ni 2p, (c) P 2p, (d) N 1s, (e) O 1s. (f) The content (%) of FeP/Fe_2P@C-200, Ni_2P@C-200, FeNiP@C, FeNiP@C-100, FeNiP@C-200 and FeNiP@C-300 M-P and C-P.

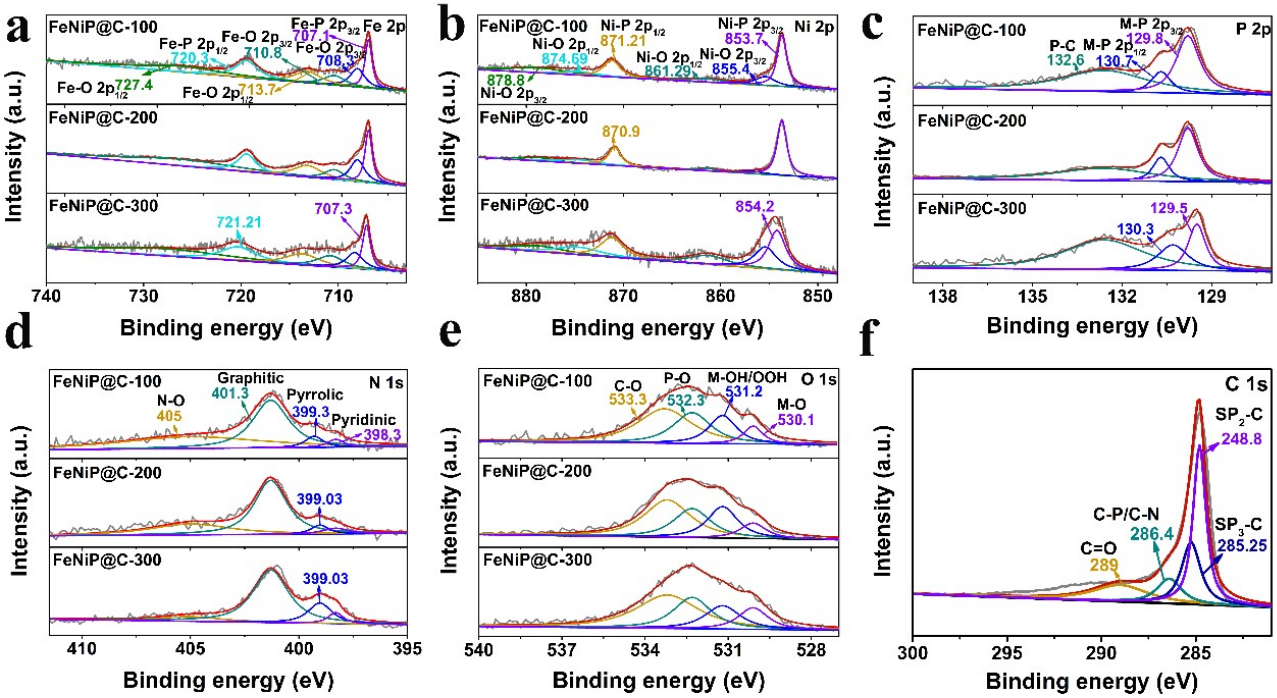

Fig. S5. XPS of FeNiP@C-100, FeNiP@C-200 and FeNiP@C-300 (a) Fe 2p, (b) Ni 2p, (c) P 2p, (d) N 1s, (e) O 1s. (f) XPS of FeP/Fe_2P@C-200, Ni_2P@C-200, FeNiP@C, FeNiP@C-100, FeNiP@C-200 and FeNiP@C-300 C 1s.

Additional electrochemical performances

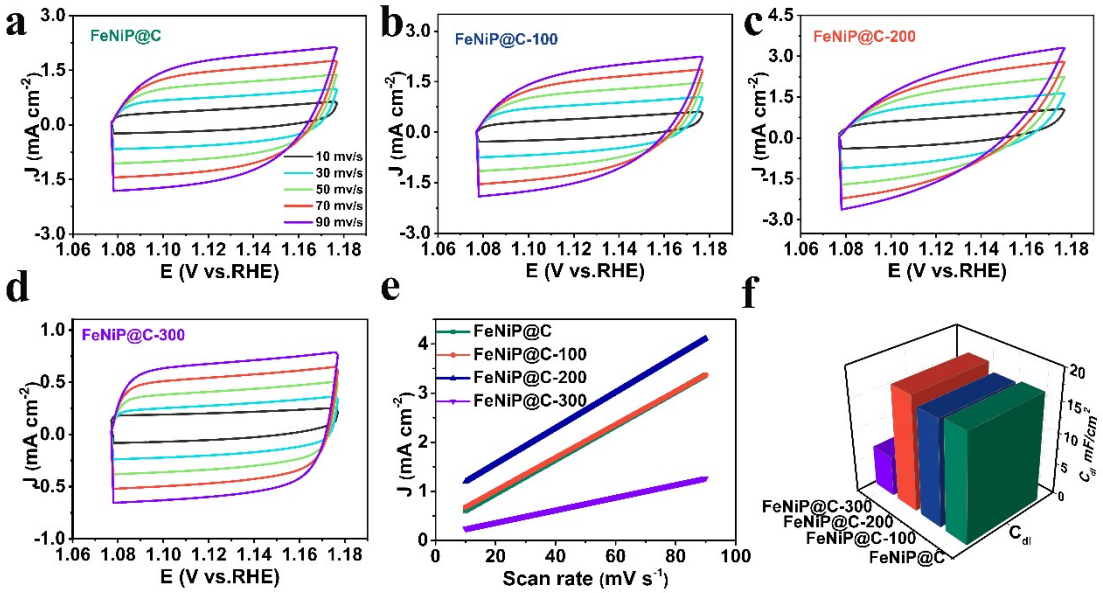

Fig. S6. (a) CV curves of FeNiP@C at different speed (10, 30, 50, 70, 90 mV/s). (b) CV curves of FeNiP@C-100 at different speed. (c) CV curves of FeNiP@C-200 at different speed. (d) CV curves of FeNiP@C-300 at different speed. (e) The corresponding plots (f) Calculated electrochemically active surface area.

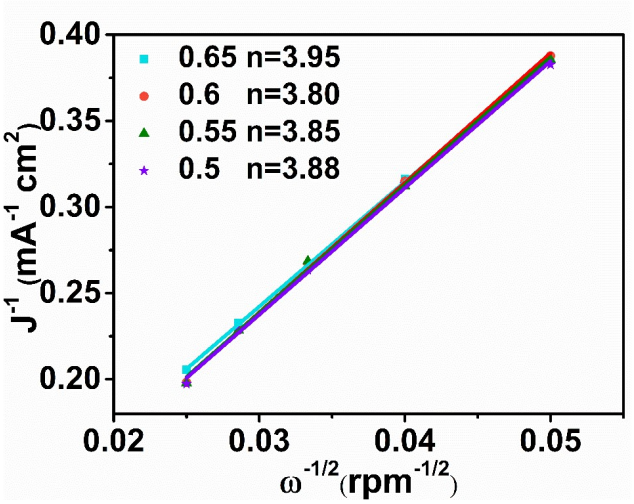

Fig. S7. The Koutecky-Levich plots of FeNiP@C-200.

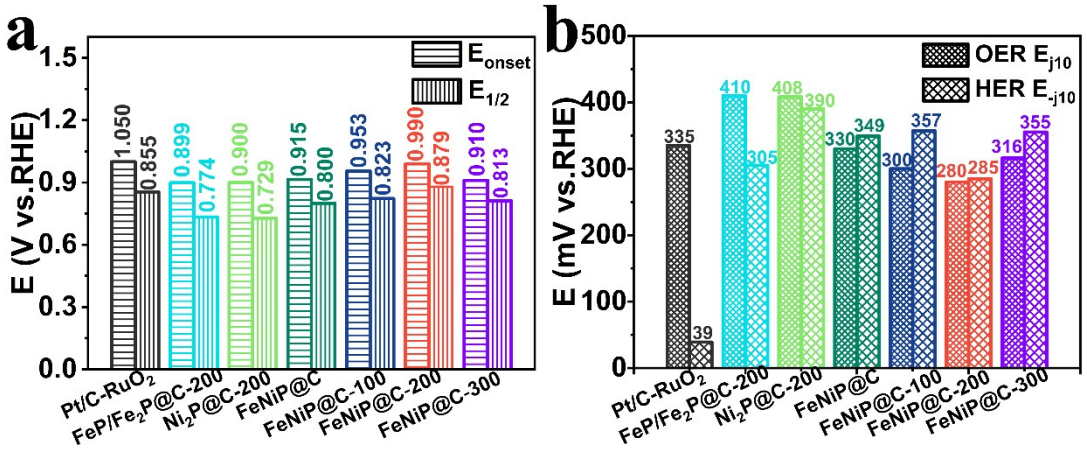

Fig. S8. (a) Comparison histogram of ORR onset potential and half-wave potential. (b) Histogram of the overpotential of OER and HER at 10 mA cm^{-2}.

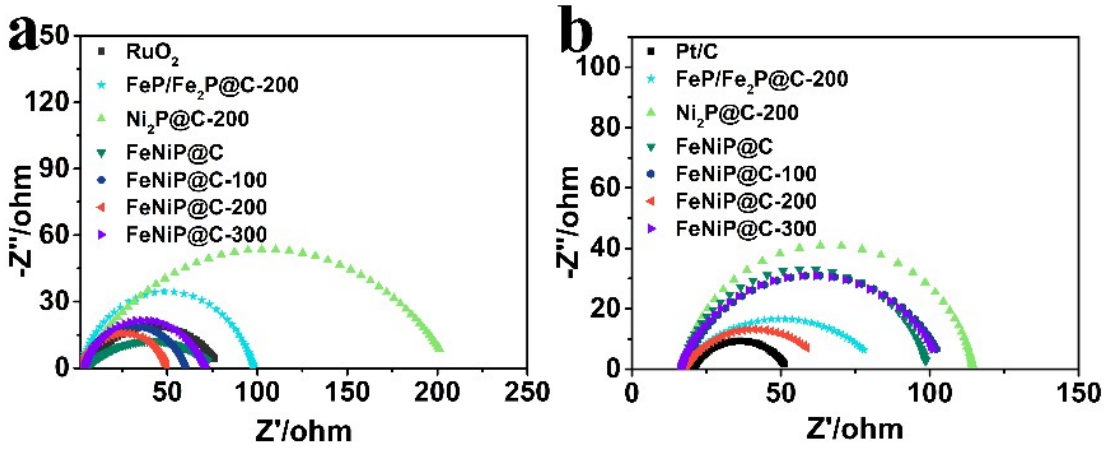

Fig. S9. (a) The electrochemical impedance of OER. (b) The electrochemical impedance of HER.

Additional battery performances

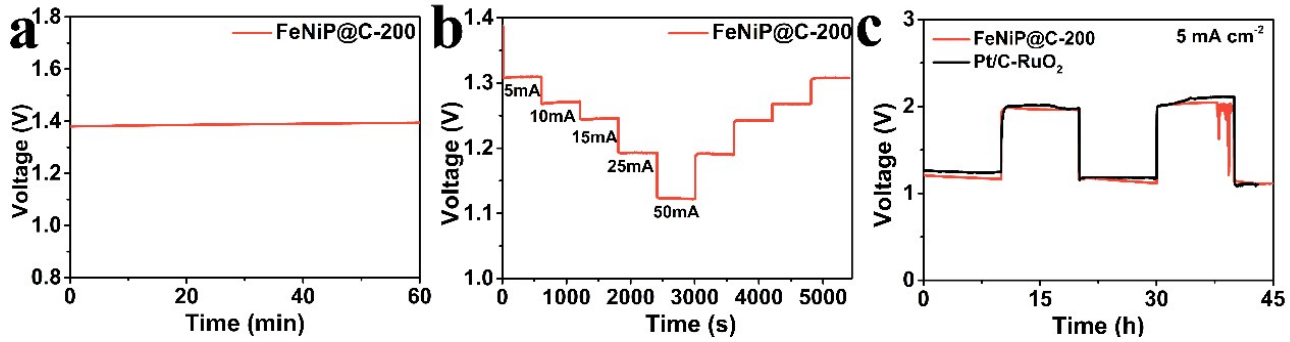

Fig. S10. (a) Open circuit voltage stability of liquid zinc-air battery. (b) Stepped discharge of liquid zinc-air battery. (c) Cycle curve of 10 h of discharge for 10 h and charge for 10 hours at a current density of 5 mA cm^{-2}.

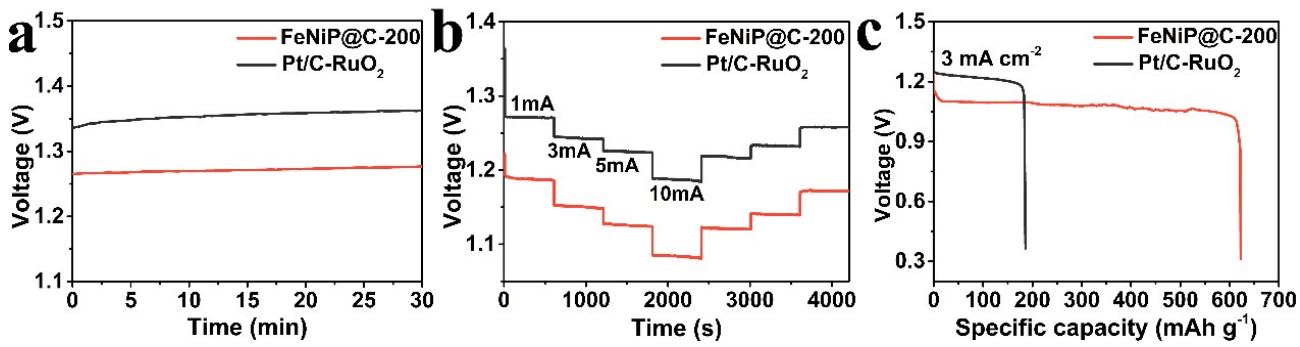

Fig. S11. (a) Open circuit voltage stability of solid zinc-air battery. (b) Stepped discharge curve of solid zinc-air battery. (c) Specific capacity of solid zinc-air battery.

Comparison of catalytic performances

Table 1. The element content of the catalyst determined by XPS

Catalysts	Fe (at%)	Ni (at%)	O (at%)	P (at%)	C (at%)	N (at%)
FeP/Fe_2P@C-200	0.58	0	5.36	1.86	89.50	2.7
Ni_2P@C-200	0	0.78	2.77	1.05	91.67	3.73
FeNiP@C	0.57	0.49	2.78	1.34	91.15	3.67
FeNiP@C-100	0.74	0.6	3.8	1.69	89.6	3.57
FeNiP@C-200	1.37	1.18	3.71	3.03	88.91	1.79
FeNiP@C-300	0.56	0.46	3.33	1.3	89.14	5.21

Table 2. Recently reported applications in electrolyzed water and zinc-air batteries on the trifunctional catalyst of ORR, OER and HER (in alkaline solution)

Catalysts	$E_{1/2}$ of ORR (V vs. RHE)	$E_{j=10}$ of OER (V vs. RHE)	$E_{j=-10}$ of HER (V vs. RHE)	$\Delta E_{OER-ORR}$ (V vs. RHE)	Ref.
FeNiP@C-200	0.879	0.28	0.285	0.70	This work
Co@N-CNTF-2	0.81	0.35	0.22	0.77	1
A-PBCCF-H	0.76	0.375	0.32	0.79	2
NSG@CNT-2	0.87	0.37	0.35	0.83	3
Co_2P/CoNPC	0.843	0.326	0.13	---	4
Co/CNT/MCP-850	0.80	0.27	0.11	---	5
Co_2P/CoN-in-NCNTs	0.85	---	0.09	0.8	6
Fe_3C-Co/NC	0.885	0.34	0.238	0.72	7
Co_9S_8@Co_9S_8@MoS_2-0.5	0.77	0.34	0.13	---	8
NCN-1000-5	0.82	0.32	---	0.81	9
CoP_x@CNS	0.76	0.286	0.091	---	10
Co/CNFs	0.896	0.32	0.19	---	11

References

1 H. Guo, Q. Feng, J. Zhu, J. Xu, Q. Li, S. Liu, K. Xu, C. Zhang, T. Liu, *J. Mater. Chem. A*, 2019, **7**, 3664-3672.
2 B. Hua, M. Li, Y.-F. Sun, Y.-Q. Zhang, N. Yan, J. Chen, T. Thundat, J. Li, J.-L. Luo, *Nano Energy*, 2017, **32**, 247-254.
3 B. Huang, X. Hu, Y. Liu, W. Qi, Z. Xie, *J. Power Sources*, 2019,**413**, 408-417.
4 H. Liu, J. Guan, S. Yang, Y. Yu, R. Shao, Z. Zhang, M. Dou, F. Wang, Q. Xu, *Adv. Mater.*, 2020, **32**, 2003649.
5 X. Zhou, X. Liu, J. Zhang, C. Zhang, S.J. Yoo, J.-G. Kim, X. Chu, C. Song, P. Wang, Z. Zhao, D. Li, W. Zhang, W. Zheng, *Carbon*, 2020, **166**, 284-290.
6 Y. Guo, P. Yuan, J. Zhang, H. Xia, F. Cheng, M. Zhou, J. Li, Y. Qiao, S. Mu, Q. Xu, *Adv. Funct. Mater.*, 2018, **28**, 1805641.
7 J. Diao, Y. Qiu, S. Liu, W. Wang, K. Chen, H. Li, W. Yuan, Y. Qu, X. Guo, *Adv. Mater.*, 2020, **32**, 1905679.
8 J. Li, G. Li, J. Wang, C. Xue, X. Li, S. Wang, B. Han, M. Yang, L. Li, *Inorg. Chem. Front.*, 2020, **7**, 191-197.
9 H. Jiang, J. Gu, X. Zheng, M. Liu, X. Qiu, L. Wang, W. Li, Z. Chen, X. Ji, J. Li, *Energy Environ. Sci.*, 2019, **12**, 322-333.
10 C.C. Hou, L. Zou, Y. Wang, Q. Xu, *Angew Chem. Int. Ed. Engl.*, 2020, **59**, 21360-21366.
11 Z. Yang, C. Zhao, Y. Qu, H. Zhou, F. Zhou, J. Wang, Y. Wu, Y. Li, Adv. Mater., 2019, **31**, 1808043.